Dynamic thin-shell black-bounce traversable wormholes

Francisco S. N. Lobo[*]

Instituto de Astrofísica e Ciências do Espaço, Faculdade de Ciências da Universidade de Lisboa,
Edifício C8, Campo Grande, P-1749-016 Lisbon, Portugal

Alex Simpson[†] and Matt Visser[‡]

School of Mathematics and Statistics, Victoria University of Wellington,
PO Box 600, Wellington 6140, New Zealand

Based on the recently introduced black-bounce spacetimes, we shall consider the construction of the related spherically symmetric thin-shell traversable wormholes within the context of standard general relativity. All of the really unusual physics is encoded in one simple parameter a which characterizes the scale of the bounce. Keeping the discussion as close as possible to standard general relativity is the theorist's version of only adjusting one feature of the model at a time. We shall modify the standard thin-shell traversable wormhole construction, each bulk region now being a black-bounce spacetime, and with the physics of the thin shell being (as much as possible) derivable from the Einstein equations. Furthermore, we shall apply a dynamical analysis to the throat by considering linearized radial perturbations around static solutions and demonstrate that the stability of the wormhole is equivalent to choosing suitable properties for the exotic material residing on the wormhole throat. The construction is sufficiently novel to be interesting and sufficiently straightforward to be tractable.

I. INTRODUCTION

One can tentatively trace back wormhole physics to Flamm's work in 1916 [1] and to the "Einstein-Rosen bridge" wormhole-type solutions considered by Einstein and Rosen (ER) in 1935 [2]. However, the field lay dormant for approximately two decades until 1955, when Wheeler became interested in topological issues in general relativity [3]. He considered multiply-connected spacetimes, where two widely separated regions were connected by a tunnel-like gravitational-electromagnetic entity, which he denoted as a "geon." These were hypothetical solutions to the coupled Einstein-Maxwell field equations. Subsequently, isolated pieces of work do appear, such as the Homer Ellis' drainhole concept [4,5], Bronnikov's tunnel-like solutions [6], and Clement's five-dimensional axisymmetric regular multiwormhole solutions [7], until the full-fledged renaissance of wormhole physics in 1988, through the seminal paper by Morris and Thorne [8].

In fact, the modern incarnation of Lorentzian wormholes (and specifically traversable wormholes) now has over 30 years of history. Early work dates from the late 1980s [8–14]. Lorentzian wormholes became considerably more mainstream in the 1990s [15–35], including work on

energy condition violations [36–42], with significant work continuing into the decades 2000–2009 [43–56] and 2010–2019 [57–70]. We shall particularly focus on the thin-shell formalism [71–76], first applied to Lorentzian wormholes in [10,11], and subsequently further developed in that and other closely related settings by many other authors [77–107]. Our notation will largely follow that of Hawking and Ellis [108]. For the purposes of this article we will focus primarily on applying the technical machinery built up regarding spherically symmetric thin-shell spacetimes in Refs. [10,26,60,61,65], and for the bulk spacetimes (away from the thin shell) shall restrict attention to the recently developed black-bounce spacetimes of Refs. [67,68] (for related work, we refer the reader to [109,110]).

Consider the following candidate regular black hole (a black bounce) specified by the spacetime line element:

$$ds^2 = -\left(1 - \frac{2m}{\sqrt{u^2 + a^2}}\right)dt^2 + \left(1 - \frac{2m}{\sqrt{u^2 + a^2}}\right)^{-1}du^2 + (u^2 + a^2)d\Omega^2. \tag{1}$$

Here the u and t coordinates have the domains $u \in (-\infty, +\infty)$ and $t \in (-\infty, +\infty)$. In the original Refs. [67,68] the u coordinate was called r; however, we now want to use the symbol r for other purposes. In this work, we shall analyze thin-shell constructions based on

[*]fslobo@fc.ul.pt
[†]alex.simpson@sms.vuw.ac.nz
[‡]matt.visser@sms.vuw.ac.nz

124035-1

this spacetime. By considering the coordinate transformation $r^2 = u^2 + a^2$, we shall use the following completely equivalent line element:

$$ds^2 = -\left(1 - \frac{2m}{r}\right)dt^2 + \left(1 - \frac{2m}{r}\right)^{-1}\left(1 - \frac{a^2}{r^2}\right)^{-1}dr^2$$
$$+ r^2 d\Omega^2. \qquad (2)$$

Here the r coordinate is now a double cover of the u coordinate. It has the domain $r \in (a, +\infty)$ and can be interpreted as the Schwarzschild area coordinate—all the 2-spheres of constant r have area $A(r) = 4\pi r^2$. This choice has the additional advantage of making it easy to directly compare the current analysis with most other work in the literature. The t coordinate has the usual domain $t \in (-\infty, +\infty)$. All of these black-bounce spacetimes are simple one-parameter modifications of Schwarzschild spacetime; for detailed analyses of the properties of these black-bounce spacetimes see Refs. [67,68].

While Lorentzian wormholes are in general very different from Mazur-Mottola gravastars [111–118], it is worth pointing out that in the thin-shell approximation there are very many technical similarities—quite often a thin-shell wormhole calculation can be modified to provide a thin-shell gravastar calculation at the cost of flipping a few strategic minus signs [119,120].

Structurally we organize the article as follows: We first introduce and briefly summarize the appropriate variant of the thin-shell formalism in Sec. II. Section III discusses some specific examples and applications. Finally we conclude in Sec. IV.

II. THIN-SHELL FORMALISM

We shall first perform a general (and relatively straightforward) theoretical analysis, somewhat along the lines laid out in Ref. [60], but with appropriate specializations, simplifications, and modifications. Subsequently we shall investigate a number of specific examples in the way of special cases and toy models. We discuss the bulk spacetimes in Sec. II A, the extrinsic curvature of the thin shells in Sec. II B, before moving on to the Lanczos equations in Sec. II C. We then discuss the Gauss and Codazzi equations in Sec. II D, before considering the equation of motion and its linearization in Secs. II E and II F. Finally we develop the master equation in Sec. II G, before moving on to the next Sec. III where we shall discuss some specific examples and applications.

A. Bulk spacetimes

We initiate the discussion by considering two distinct "bulk" spacetime manifolds, $\mathcal{M}_+$ and $\mathcal{M}_-$, equipped with boundaries $\partial\mathcal{M}_+ = \Sigma_+$ and $\partial\mathcal{M}_- = \Sigma_-$. As long as the boundaries are isometric, $\Sigma_+ \sim \Sigma_-$, then we can define a manifold $\mathcal{M} = \mathcal{M}_+ \cup \mathcal{M}_-$, which is smooth except

possibly for a thin-shell transition layer at $\Sigma_+ \sim \Sigma_-$. In particular, consider two static spherically symmetric black-bounce spacetimes given on $\mathcal{M}_\pm$ by the following two-parameter (m, a) Lorentzian-signature line elements $g^+_{\mu\nu}(x^\mu_+)$ and $g^-_{\mu\nu}(x^\mu_-)$:

$$ds^2 = -\left(1 - \frac{2m_\pm}{r_\pm}\right)dt^2_\pm + \left(1 - \frac{2m_\pm}{r_\pm}\right)^{-1}\left(1 - \frac{a^2_\pm}{r^2_\pm}\right)^{-1}dr^2_\pm$$
$$+ r^2_\pm d\Omega^2_\pm. \qquad (3)$$

The usual Einstein field equations, $G_{\mu\nu} = 8\pi T_{\mu\nu}$ (with $c = G = 1$), imply that the physically relevant orthonormal components of the stress-energy tensor are (in the two bulk regions) specified by

$$\rho(r) = -\frac{1}{8\pi}\frac{a^2(r - 4m)}{r^5}, \qquad (4)$$

$$p_r(r) = -\frac{1}{8\pi}\frac{a^2}{r^4}, \qquad (5)$$

$$p_t(r) = \frac{1}{8\pi}\frac{a^2(r - m)}{r^5}. \qquad (6)$$

Here $\rho(r)$ is the energy density, $p_r(r)$ is the radial pressure, and $p_t(r)$ is the transverse pressure. Given the spherical symmetry, $p_t(r)$ is the pressure measured in the two directions orthogonal to the radial direction. The subscripts $\pm$ (on $m_\pm$ and $a_\pm$) have been (temporarily) suppressed for clarity.

The null energy condition (NEC) is satisfied provided, for any arbitrary null vector k^a, the stress energy $T_{\mu\nu}$ satisfies $T_{\mu\nu}k^\mu k^\nu \geq 0$. The radial null vector is $k^{\hat{\mu}} = (1, \pm1, 0, 0)$ in the orthonormal frame where the stress energy is $T_{\hat{\mu}\hat{\nu}} = \text{diag}[\rho(r), p_r(r), p_t(r), p_t(r)]$. Then

$$(T_{\hat{\mu}\hat{\nu}}k^{\hat{\mu}}k^{\hat{\nu}})_{\text{radial}} = \rho(r) + p_r(r) = -\frac{a^2(r - 2m)}{4\pi r^5} < 0. \qquad (7)$$

To verify the negativity of this quantity, note that the bulk spacetime models a regular black hole when $a \in (0, 2m)$, with horizons at $u_H = \pm\sqrt{(2m)^2 - a^2}$, corresponding to $r_H = u_H^2 + a^2 = 2m$. We therefore "chop" the spacetime outside any horizons that are present. Hence in both of the bulk regions we have the condition that $r > 2m$. Thus the radial NEC will be manifestly violated in both of the bulk regions of the black-bounce thin-shell spacetime. In the context of static spherical symmetry, this is sufficient to conclude that all of the standard energy conditions associated with general relativistic analysis will be similarly violated.

In the transverse directions we can choose the null vector to be $k^{\hat{\mu}} = (1, 0, \cos\zeta, \sin\zeta)$ and so

$$(T_{\hat{\mu}\hat{\nu}}k^{\hat{\mu}}k^{\hat{\nu}})_{\text{transverse}} = \rho(r) + p_t(r) = \frac{3a^2 m}{8\pi r^5} > 0. \quad (8)$$

While this is manifestly positive, this is not enough to override the NEC violations coming from the radial direction.

B. Normal 4-vector and extrinsic curvature

The two bulk manifolds, $\mathcal{M}_+$ and $\mathcal{M}_-$, are bounded by the hypersurfaces $\partial\mathcal{M}_+ = \Sigma_+$ and $\mathcal{M}_- = \Sigma_-$. These two hypersurfaces possess induced 3-metrics g_{ij}^+ and g_{ij}^-, respectively. The $\Sigma_\pm$ are chosen to be isometric. [In terms of the intrinsic coordinates, $g_{ij}^\pm(\xi) = g_{ij}(\xi)$, with $\xi^i = (\tau, \theta, \phi)$.] Thence a single manifold $\mathcal{M}$ is obtained by gluing together $\mathcal{M}_+$ and $\mathcal{M}_-$ at their boundaries, that is, $\mathcal{M} = \mathcal{M}_+ \cup \mathcal{M}_-$, with the natural identification of the two boundaries $\Sigma_\pm = \Sigma$.

The boundary manifold Σ possesses three tangent basis vectors $\mathbf{e}_{(i)} = \partial/\partial\xi^i$, with the holonomic components $e_{(i)}^\mu|_\pm = \partial x_\pm^\mu/\partial\xi^i$. This basis specifies the induced metric via the scalar product $g_{ij} = \mathbf{e}_{(i)} \cdot \mathbf{e}_{(j)} = g_{\mu\nu}e_{(i)}^\mu e_{(j)}^\nu|_\pm$. Finally, in explicit coordinates, the intrinsic metric to Σ is given by

$$ds_\Sigma^2 = -d\tau^2 + R^2(\tau)(d\theta^2 + \sin^2\theta d\phi^2). \quad (9)$$

That is, the manifold $\mathcal{M}$ is obtained by gluing $\mathcal{M}_+$ and $\mathcal{M}_-$ at the 3-surface $x^\mu(\tau, \theta, \phi) = (t(\tau), R(\tau), \theta, \phi)$. The respective 4-velocities, tangent to the junction surface and orthogonal to the slices of spherical symmetry, are defined on the two sides of the junction surface. They are explicitly given by

$$U_\pm^\mu = \left(\frac{\sqrt{\left(1 - \frac{2m_\pm}{R}\right)\left(1 - \frac{a_\pm^2}{R^2}\right) + \dot{R}^2}}{\left(1 - \frac{2m_\pm}{R}\right)\left(1 - \frac{a_\pm^2}{R^2}\right)^{1/2}}, \dot{R}, 0, 0 \right). \quad (10)$$

Here τ is the proper time of an observer comoving with Σ, and the overdot denotes a derivative with respect to this proper time. Furthermore, the timelike junction surface Σ is given by the parametric equation $f(x^\mu(\xi^i)) = r - a(\tau) = 0$, and the unit normal 4-vector, n^μ, is defined as

$$n_\mu = \frac{\nabla_a f}{\|\nabla f\|} = \pm \left| g^{\alpha\beta}\frac{\partial f}{\partial x^\alpha}\frac{\partial f}{\partial x^\beta} \right|^{-1/2}\frac{\partial f}{\partial x^\mu}. \quad (11)$$

Hence $n_\mu n^\mu = +1$ and $n_\mu e_{(i)}^\mu = 0$. In the usual Israel formalism one chooses the normals to point from $\mathcal{M}_-$ to $\mathcal{M}_+$ [76], so that the unit normals to the junction surface are provided by the following expressions:

$$n_\pm^\mu = \pm \left(\frac{\dot{R}}{\left(1 - \frac{2m_\pm}{R}\right)\left(1 - \frac{a_\pm^2}{R^2}\right)^{1/2}}, \right.$$
$$\left. \sqrt{\left(1 - \frac{2m_\pm}{R}\right)\left(1 - \frac{a_\pm^2}{R^2}\right) + \dot{R}^2}, 0, 0 \right). \quad (12)$$

Taking into account spherical symmetry one may also obtain the above expressions from consideration of the contractions $U^\mu n_\mu = 0$ and $n^\mu n_\mu = +1$. The extrinsic curvature, or second fundamental form, is typically defined as $K_{ij} = n_{(\mu;\nu)}e_{(i)}^\mu e_{(j)}^\nu$. Now, by differentiating $n_\mu e_{(i)}^\mu = 0$ with respect to ξ^j, one obtains the following useful relation:

$$n_\mu \frac{\partial^2 x^\mu}{\partial\xi^i\partial\xi^j} = -n_{\mu,\nu}\frac{\partial x^\mu}{\partial\xi^i}\frac{\partial x^\nu}{\partial\xi^j}, \quad (13)$$

so that the extrinsic curvature K_{ij} can therefore be represented in the form

$$K_{ij}^\pm = -n_\mu \left(\frac{\partial^2 x^\mu}{\partial\xi^i\partial\xi^j} + \Gamma_{\alpha\beta}^{\mu\pm}\frac{\partial x^\alpha}{\partial\xi^i}\frac{\partial x^\beta}{\partial\xi^j} \right). \quad (14)$$

Finally, using both spherical symmetry and Eq. (14), the nontrivial components of the extrinsic curvature are given by

$$K^\theta_{\ \theta}^\pm = \pm\frac{1}{R}\sqrt{\left(1 - \frac{2m_\pm}{R}\right)\left(1 - \frac{a_\pm^2}{R^2}\right) + \dot{R}^2}, \quad (15)$$

$$K^\tau_{\ \tau}^\pm = \pm \left[\frac{\ddot{R} - \frac{a_\pm^2}{R(R^2-a_\pm^2)}\dot{R}^2 + \frac{m_\pm(R^2-a_\pm^2)}{R^4}}{\sqrt{\left(1 - \frac{2m_\pm}{R}\right)\left(1 - \frac{a_\pm^2}{R^2}\right) + \dot{R}^2}} \right]. \quad (16)$$

C. Lanczos equations and surface stress energy

For the case of a thin shell, the extrinsic curvature need not be continuous across Σ. For notational clarity we denote the discontinuity in K_{ij} as $\kappa_{ij} = K_{ij}^+ - K_{ij}^-$. The Einstein equations, when applied to the hypersurface joining the bulk spacetimes, now yield the Lanczos equations:

$$S^i_{\ j} = -\frac{1}{8\pi}(\kappa^i_{\ j} - \delta^i_{\ j}\kappa^k_{\ k}), \quad (17)$$

where $S^i_{\ j}$ is the surface stress-energy tensor on the junction interface Σ. Because of spherical symmetry $\kappa^i_{\ j} = \text{diag}(\kappa^\tau_{\ \tau}, \kappa^\theta_{\ \theta}, \kappa^\theta_{\ \theta})$, the surface stress-energy tensor reduces to $S^i_{\ j} = \text{diag}(-\sigma, \mathcal{P}, \mathcal{P})$, where σ is the surface energy density, and $\mathcal{P}$ the surface pressure. The Lanczos equations imply

$$\sigma = -\frac{1}{4\pi}\kappa^\theta{}_\theta, \tag{18}$$

$$\mathcal{P} = \frac{1}{8\pi}(\kappa^\tau{}_\tau + \kappa^\theta{}_\theta). \tag{19}$$

Using the computed extrinsic curvatures (15) and (16), we now evaluate the surface stresses:

$$\sigma = -\frac{1}{4\pi R}\left[\sqrt{\left(1-\frac{2m_+}{R}\right)\left(1-\frac{a_+^2}{R^2}\right)+\dot{R}^2}\right.$$
$$\left.+\sqrt{\left(1-\frac{2m_-}{R}\right)\left(1-\frac{a_-^2}{R^2}\right)+\dot{R}^2}\right], \tag{20}$$

$$\mathcal{P} = \frac{1}{8\pi R}\left[\frac{1+\dot{R}^2\left(\frac{R^2-2a_+^2}{R^2-a_+^2}\right)+R\ddot{R}-\frac{m_+R^2+a_+^2(R-m_+)}{R^3}}{\sqrt{\left(1-\frac{2m_+}{R}\right)\left(1-\frac{a_+^2}{R^2}\right)+\dot{R}^2}}\right.$$
$$\left.+\frac{1+\dot{R}^2\left(\frac{R^2-2a_-^2}{R^2-a_-^2}\right)+R\ddot{R}-\frac{m_-R^2+a_-^2(R-m_-)}{R^3}}{\sqrt{\left(1-\frac{2m_-}{R}\right)\left(1-\frac{a_-^2}{R^2}\right)+\dot{R}^2}}\right]. \tag{21}$$

The surface mass of the thin shell is defined by $m_s = 4\pi R^2\sigma$, a result that we shall use extensively below. Furthermore the surface energy density σ is always negative, implying energy condition violations in this thin-shell context. For the specific symmetric case, $m_+ = m_-$, and for vanishing bounce parameters $a_\pm = 0$, the analysis reduces to that of Ref. [25].

D. Gauss and Codazzi equations

The Gauss equation is sometimes called the first contracted Gauss-Codazzi equation. In standard general relativity it is more often referred to as the "Hamiltonian constraint." The Gauss equation is a purely mathematical statement relating bulk curvature to extrinsic and intrinsic curvature at the boundary:

$$G_{\mu\nu}n^\mu n^\nu = \frac{1}{2}(K^2 - K_{ij}K^{ij} - {}^3R). \tag{22}$$

Applying the Einstein equation, and evaluating the discontinuity across the junction surface, this becomes

$$8\pi[T_{\mu\nu}n^\mu n^\nu]_-^+ = \frac{1}{2}[K^2 - K_{ij}K^{ij}]. \tag{23}$$

Using the conventions $[X]_-^+ \equiv X^+|_\Sigma - X^-|_\Sigma$ and $\bar{X} \equiv \frac{1}{2}(X^+|_\Sigma + X^-|_\Sigma)$ for notational simplicity, and applying the Lanczos equations, one deduces the constraint equation

$$[T_{\mu\nu}n^\mu n^\nu]_-^+ = S^{ij}\bar{K}_{ij}. \tag{24}$$

In contrast the Codazzi equation (Codazzi-Mainardi equation) is often known as the second contracted Gauss-Codazzi equation. In general relativity it is more often referred to as the "ADM constraint" or "momentum constraint." The purely mathematical result is

$$G_{\mu\nu}e^\mu_{(i)}n^\nu = K^j_{i|j} - K_{,i}. \tag{25}$$

Together with the Einstein and Lanczos equations, and considering the discontinuity across the thin shell, this now yields the conservation identity:

$$[T_{\mu\nu}e^\mu_{(j)}n^\nu]_-^+ = -S^i_{j|i}. \tag{26}$$

The left-hand side of the conservation identity (26) can be interpreted in terms of momentum flux. Explicitly

$$[T_{\mu\nu}e^\mu_{(\tau)}n^\nu]_-^+$$
$$= [T_{\mu\nu}U^\mu n^\nu]_-^+$$
$$= \left[\pm(T_{\hat{t}\hat{t}} + T_{\hat{r}\hat{r}})\frac{\dot{R}\sqrt{(1-\frac{2m}{R})(1-\frac{a^2}{R^2})+\dot{R}^2}}{(1-\frac{2m}{R})(1-\frac{a^2}{R^2})}\right]_-^+$$
$$= \left[\mp\frac{a^2}{4\pi R^4}\frac{\dot{R}\sqrt{(1-\frac{2m}{R})(1-\frac{a^2}{R^2})+\dot{R}^2}}{(1-\frac{a^2}{R^2})}\right]_-^+, \tag{27}$$

where $T_{\hat{t}\hat{t}}$ and $T_{\hat{r}\hat{r}}$ are the bulk stress-energy tensor components given in an orthonormal basis. Note that the flux term corresponds to the net discontinuity in the bulk momentum flux $F_\mu = T_{\mu\nu}U^\nu$ which impinges on the shell. For notational simplicity, we write

$$[T_{\mu\nu}e^\mu_{(\tau)}n^\nu]_-^+ = \dot{R}\Xi. \tag{28}$$

Here we have defined the useful quantity

$$\Xi = -\frac{1}{4\pi R^2}\left[\frac{a_+^2}{(R^2-a_+^2)}\sqrt{\left(1-\frac{2m_+}{R}\right)\left(1-\frac{a_+^2}{R^2}\right)+\dot{R}^2}\right.$$
$$\left.+\frac{a_-^2}{(R^2-a_-^2)}\sqrt{\left(1-\frac{2m_-}{R}\right)\left(1-\frac{a_-^2}{R^2}\right)+\dot{R}^2}\right]. \tag{29}$$

Now $A = 4\pi R^2$ is the surface area of the thin shell. The conservation identity becomes

$$\frac{d\sigma}{d\tau} + (\sigma + \mathcal{P})\frac{1}{A}\frac{dA}{d\tau} = \Xi\dot{R}. \tag{30}$$

Equivalently

$$\frac{d(\sigma A)}{d\tau} + \mathcal{P}\frac{dA}{d\tau} = \Xi A \dot{R}. \tag{31}$$

The term on the right-hand side incorporates the flux term and encodes the work done by external forces, while the first term on the left-hand side is simply the variation of the internal energy of the shell, and the second term characterizes the work done by the shell's internal forces. Provided that the equations of motion can be integrated to determine the surface energy density as a function of radius R we infer the existence of a suitable function $\sigma(R)$. Defining $\sigma' = d\sigma/dR$ the conservation equation can then be written as

$$\sigma' = -\frac{2}{R}(\sigma + \mathcal{P}) + \Xi. \tag{32}$$

E. Equation of motion

To analyze the stability of the wormhole, Eq. (20) can be rearranged to provide the thin-shell equation of motion, given by

$$\frac{1}{2}\dot{R}^2 + V(R) = 0. \tag{33}$$

The potential $V(R)$ is defined as

$$V(R) = \frac{1}{2}\left\{1 - \frac{\bar{\Delta}(R)}{R} - \left[\frac{m_s(R)}{2R}\right]^2 - \left[\frac{\Delta(R)}{m_s(R)}\right]^2\right\}, \tag{34}$$

where $m_s(R) = 4\pi R^2 \sigma(R)$ is the mass of the thin shell, and the quantities $\bar{\Delta}(R)$ and $\Delta(R)$ are defined as

$$\bar{\Delta}(R) = (m_+ + m_-)$$
$$+ \frac{1}{2R}\left[a_+^2\left(1 - \frac{2m_+}{R}\right) + a_-^2\left(1 - \frac{2m_-}{R}\right)\right], \tag{35}$$

$$\Delta(R) = (m_+ - m_-)$$
$$+ \frac{1}{2R}\left[a_+^2\left(1 - \frac{2m_+}{R}\right) - a_-^2\left(1 - \frac{2m_-}{R}\right)\right], \tag{36}$$

respectively. Note that by differentiating with respect to τ, the equation of motion implies $\ddot{R} = -V'(R)$, which will be useful below.

As outlined in Ref. [60], we can reverse the logic flow and determine the surface mass as a function of the potential. More specifically, if we impose a specific potential $V(R)$, this potential implicitly tells us how much surface mass we need to distribute on the wormhole throat. This further places implicit demands on the equation of state of the exotic matter residing on the wormhole throat. This implies that, after imposing the equation of motion for the shell, one has the following:

Surface energy density:

$$\sigma = -\frac{1}{4\pi R}\left[\sqrt{\left(1 - \frac{2m_+}{R}\right)\left(1 - \frac{a_+^2}{R^2}\right) - 2V(R)}\right.$$
$$\left. + \sqrt{\left(1 - \frac{2m_-}{R}\right)\left(1 - \frac{a_-^2}{R^2}\right) - 2V(R)}\right]. \tag{37}$$

Surface pressure:

$$\mathcal{P} = \frac{1}{8\pi R}\left[\frac{1 - 2V(R)\left(\frac{R^2 - 2a_+^2}{R^2 - a_+^2}\right) - RV'(R) - \frac{m_+ R^2 + a_+^2(R - m_+)}{R^3}}{\sqrt{\left(1 - \frac{2m_+}{R}\right)\left(1 - \frac{a_+^2}{R^2}\right) - 2V(R)}}\right.$$
$$\left. + \frac{1 - 2V(R)\left(\frac{R^2 - 2a_-^2}{R^2 - a_-^2}\right) - RV'(R) - \frac{m_- R^2 + a_-^2(R - m_-)}{R^3}}{\sqrt{\left(1 - \frac{2m_-}{R}\right)\left(1 - \frac{a_-^2}{R^2}\right) - 2V(R)}}\right]. \tag{38}$$

External energy flux:

$$\Xi = -\frac{1}{4\pi R^2}\left[\frac{a_+^2}{(R^2 - a_+^2)}\sqrt{\left(1 - \frac{2m_+}{R}\right)\left(1 - \frac{a_+^2}{R^2}\right) - 2V(R)}\right.$$
$$\left. + \frac{a_-^2}{(R^2 - a_-^2)}\sqrt{\left(1 - \frac{2m_-}{R}\right)\left(1 - \frac{a_-^2}{R^2}\right) - 2V(R)}\right]. \tag{39}$$

These three quantities, $\{\sigma(R), \mathcal{P}(R), \Xi(R)\}$, are interrelated by the differential conservation law, so at most two of them are functionally independent. We could equivalently work with the quantities $\{m_s(R), \mathcal{P}(R), \Xi(R)\}$.

F. Linearized equation of motion

We now consider the equation of motion $\frac{1}{2}\dot{R}^2 + V(R) = 0$, which implies $\ddot{R} = -V'(R)$, and linearize around an assumed static solution at R_0. This implies that a second-order Taylor expansion of $V(R)$ around R_0 provides

$$V(R) = V(R_0) + V'(R_0)(R - R_0) + \frac{1}{2}V''(R_0)(R - R_0)^2$$
$$+ O[(R - R_0)^3]. \tag{40}$$

Since we are expanding around a static solution, $\dot{R}_0 = \ddot{R}_0 = 0$, we have both $V(R_0) = V'(R_0) = 0$, so that Eq. (40) reduces to

$$V(R) = \frac{1}{2}V''(R_0)(R - R_0)^2 + O[(R - R_0)^3]. \tag{41}$$

The static solution at R_0 is stable if and only if $V(R)$ has a local minimum at R_0. This requires $V''(R_0) > 0$. This stability condition will be our fundamental tool in the subsequent analysis—though reformulation in terms of more basic quantities will prove useful. For instance, it is useful to express the quantities $m_s'(R)$ and $m_s''(R)$ in terms of the potential and its derivatives—doing so allows us to develop a simple inequality on $m_s''(R_0)$ by using the constraint $V''(R_0) > 0$. Similar formulas will hold for the pairs $\sigma'(R)$, $\sigma''(R)$, for $\mathcal{P}'(R)$, $\mathcal{P}''(R)$, and for $\Xi'(R)$, $\Xi''(R)$. In view of the multiple redundancies coming from the relations $m_s(R) = 4\pi\sigma(R)R^2$ and the differential conservation law, we can easily see that the only interesting quantities are $\Xi'(R)$, $\Xi''(R)$.

In the applications analyzed below, it is extremely useful to consider the dimensionless quantity

$$\frac{m_s(R)}{R} = 4\pi\sigma(R)R = -\left[\sqrt{\left(1 - \frac{2m_+}{R}\right)\left(1 - \frac{a_+^2}{R^2}\right) - 2V(R)} + \sqrt{\left(1 - \frac{2m_-}{R}\right)\left(1 - \frac{a_-^2}{R^2}\right) - 2V(R)}\right]. \tag{42}$$

We now express $[m_s(R)/R]'$ and $[m_s(R)/R]''$ in terms of the following quantities:

$$\left[\frac{m_s(R)}{R}\right]' = -\left\{\frac{\frac{m_+}{R^2}\left(1 - \frac{a_+^2}{R^2}\right) + \frac{a_+^2}{R^3}\left(1 - \frac{2m_+}{R}\right) - V'(R)}{\sqrt{\left(1 - \frac{2m_+}{R}\right)\left(1 - \frac{a_+^2}{R^2}\right) - 2V(R)}} + \frac{\frac{m_-}{R^2}\left(1 - \frac{a_-^2}{R^2}\right) + \frac{a_-^2}{R^3}\left(1 - \frac{2m_-}{R}\right) - V'(R)}{\sqrt{\left(1 - \frac{2m_-}{R}\right)\left(1 - \frac{a_-^2}{R^2}\right) - 2V(R)}}\right\} \tag{43}$$

and

$$\left[\frac{m_s(R)}{R}\right]'' = \left\{\frac{\left[\frac{m_+}{R^2}\left(1 - \frac{a_+^2}{R^2}\right) + \frac{a_+^2}{R^3}\left(1 - \frac{2m_+}{R}\right) - V'(a)\right]^2}{\left[\left(1 - \frac{2m_+}{R}\right)\left(1 - \frac{a_+^2}{R^2}\right) - 2V(R)\right]^{3/2}} + \frac{\frac{2m_+}{R^3}\left(1 - \frac{a_+^2}{R^2}\right) + \frac{3a_+^2}{R^4}\left(1 - \frac{2m_+}{R}\right) - \frac{4m_+ a_+^2}{R^5} + V''(R)}{\sqrt{\left(1 - \frac{2m_+}{R}\right)\left(1 - \frac{a_+^2}{R^2}\right) - 2V(R)}}\right.$$
$$\left. + \frac{\left[\frac{m_-}{R^2}\left(1 - \frac{a_-^2}{R^2}\right) + \frac{a_-^2}{R^3}\left(1 - \frac{2m_-}{R}\right) - V'(R)\right]^2}{\left[\left(1 - \frac{2m_-}{R}\right)\left(1 - \frac{a_-^2}{R^2}\right) - 2V(R)\right]^{3/2}} + \frac{\frac{2m_-}{R^3}\left(1 - \frac{a_-^2}{R^2}\right) + \frac{3a_-^2}{R^4}\left(1 - \frac{2m_-}{R}\right) - \frac{4m_- a_-^2}{R^5} + V''(R)}{\sqrt{\left(1 - \frac{2m_-}{R}\right)\left(1 - \frac{a_-^2}{R^2}\right) - 2V(R)}}\right\}. \tag{44}$$

Similarly, consider the useful dimensionless quantity

$$4\pi R^2 \Xi = -\left[\frac{a_+^2}{(R^2 - a_+^2)}\sqrt{\left(1 - \frac{2m_+}{R}\right)\left(1 - \frac{a_+^2}{R^2}\right) - 2V(R)} + \frac{a_-^2}{(R^2 - a_-^2)}\sqrt{\left(1 - \frac{2m_-}{R}\right)\left(1 - \frac{a_-^2}{R^2}\right) - 2V(R)}\right]. \tag{45}$$

This leads to the following relations:

$$[4\pi R^2 \Xi]' = \frac{a_+^2}{(R^2 - a_+^2)}\left[\frac{2R}{(R^2 - a_+^2)}\sqrt{\left(1 - \frac{2m_+}{R}\right)\left(1 - \frac{a_+^2}{R^2}\right) - 2V(R)} - \frac{\frac{m_+}{R^2}\left(1 - \frac{a_+^2}{R^2}\right) + \frac{a_+^2}{R^3}\left(1 - \frac{2m_+}{R}\right) - V'(R)}{\sqrt{\left(1 - \frac{2m_+}{R}\right)\left(1 - \frac{a_+^2}{R^2}\right) - 2V(R)}}\right]$$
$$+ \frac{a_-^2}{(R^2 - a_-^2)}\left[\frac{2R}{(R^2 - a_-^2)}\sqrt{\left(1 - \frac{2m_-}{R}\right)\left(1 - \frac{a_-^2}{R^2}\right) - 2V(R)} - \frac{\frac{m_-}{R^2}\left(1 - \frac{a_-^2}{R^2}\right) + \frac{a_-^2}{R^3}\left(1 - \frac{2m_-}{R}\right) - V'(R)}{\sqrt{\left(1 - \frac{2m_-}{R}\right)\left(1 - \frac{a_-^2}{R^2}\right) - 2V(R)}}\right] \tag{46}$$

and

$$
\begin{aligned}
[4\pi R^2 \Xi]'' = & \left\{ -\frac{2a_+^2(3R^2+a_+^2)}{(R^2-a_+^2)^3}\sqrt{\left(1-\frac{2m_+}{R}\right)\left(1-\frac{a_+^2}{R^2}\right)-2V(R)} + \frac{4a_+^2 R}{(R^2-a_+^2)^2}\frac{\frac{m_+}{R^2}\left(1-\frac{a_+^2}{R^2}\right)+\frac{a_+^2}{R^3}\left(1-\frac{2m_+}{R}\right)-V'(R)}{\sqrt{\left(1-\frac{2m_+}{R}\right)\left(1-\frac{a_+^2}{R^2}\right)-2V(R)}} \right. \\
& + \frac{a_+^2}{(R^2-a_+^2)}\frac{\left[\frac{m_+}{R^2}\left(1-\frac{a_+^2}{R^2}\right)+\frac{a_+^2}{R^3}\left(1-\frac{2m_+}{R}\right)-V'(R)\right]^2}{\left[\left(1-\frac{2m_+}{R}\right)\left(1-\frac{a_+^2}{R^2}\right)-2V(R)\right]^{3(2}} \\
& \left. + \frac{a_+^2}{(R^2-a_+^2)}\frac{\frac{2m_+}{R^3}\left(1-\frac{a_+^2}{R^2}\right)+\frac{3a_+^2}{R^4}\left(1-\frac{2m_+}{R}\right)-\frac{4m_+a_+^2}{R^5}+V''(R)}{\sqrt{\left(1-\frac{2m_+}{R}\right)\left(1-\frac{a_+^2}{R^2}\right)-2V(R)}} \right\} \\
& + \left\{ -\frac{2a_-^2(3R^2+a_-^2)}{(R^2-a_-^2)^3}\sqrt{\left(1-\frac{2m_-}{R}\right)\left(1-\frac{a_-^2}{R^2}\right)-2V(R)} + \frac{4a_-^2 R}{(R^2-a_-^2)^2}\frac{\frac{m_-}{R^2}\left(1-\frac{a_-^2}{R^2}\right)+\frac{a_-^2}{R^3}\left(1-\frac{2m_-}{R}\right)-V'(R)}{\sqrt{\left(1-\frac{2m_-}{R}\right)\left(1-\frac{a_-^2}{R^2}\right)-2V(R)}} \right. \\
& + \frac{a_-^2}{(R^2-a_-^2)}\frac{\left[\frac{m_-}{R^2}\left(1-\frac{a_-^2}{R^2}\right)+\frac{a_-^2}{R^3}\left(1-\frac{2m_-}{R}\right)-V'(R)\right]^2}{\left[\left(1-\frac{2m_-}{R}\right)\left(1-\frac{a_-^2}{R^2}\right)-2V(R)\right]^{3(2}} \\
& \left. + \frac{a_-^2}{(R^2-a_-^2)}\frac{\frac{2m_-}{R^3}\left(1-\frac{a_-^2}{R^2}\right)+\frac{3a_-^2}{R^4}\left(1-\frac{2m_-}{R}\right)-\frac{4m_-a_-^2}{R^5}+V''(R)}{\sqrt{\left(1-\frac{2m_-}{R}\right)\left(1-\frac{a_-^2}{R^2}\right)-2V(R)}} \right\}.
\end{aligned}
\tag{47}
$$

G. Master equation

Taking into account the extensive discussion above, we see that to have a stable static solution at R_0, we must satisfy two equations and one inequality. Specifically,

$$
\frac{m_s(R_0)}{R_0} = 4\pi\sigma(R_0)R_0 = -\left[\sqrt{\left(1-\frac{2m_+}{R_0}\right)\left(1-\frac{a_+^2}{R_0^2}\right)}+\sqrt{\left(1-\frac{2m_-}{R_0}\right)\left(1-\frac{a_-^2}{R_0^2}\right)}\right],
\tag{48}
$$

and

$$
\left[\frac{m_s(R_0)}{R_0}\right]' = -\left\{\frac{\frac{m_+}{R_0^2}\left(1-\frac{a_+^2}{R_0^2}\right)+\frac{a_+^2}{R_0^3}\left(1-\frac{2m_+}{R_0}\right)}{\sqrt{\left(1-\frac{2m_+}{R_0}\right)\left(1-\frac{a_+^2}{R_0^2}\right)}}+\frac{\frac{m_-}{R_0^2}\left(1-\frac{a_-^2}{R_0^2}\right)+\frac{a_-^2}{R_0^3}\left(1-\frac{2m_-}{R_0}\right)}{\sqrt{\left(1-\frac{2m_-}{R_0}\right)\left(1-\frac{a_-^2}{R_0^2}\right)}}\right\},
\tag{49}
$$

and

$$
\begin{aligned}
\left[\frac{m_s(R_0)}{R_0}\right]'' \geq & \left\{\frac{\left[\frac{m_+}{R_0^2}\left(1-\frac{a_+^2}{R_0^2}\right)+\frac{a_+^2}{R_0^3}\left(1-\frac{2m_+}{R_0}\right)\right]^2}{\left[\left(1-\frac{2m_+}{R_0}\right)\left(1-\frac{a_+^2}{R_0^2}\right)\right]^{3/2}}+\frac{\frac{2m_+}{R_0^3}\left(1-\frac{a_+^2}{R_0^2}\right)+\frac{3a_+^2}{R_0^4}\left(1-\frac{2m_+}{R_0}\right)-\frac{4m_+a_+^2}{R_0^5}}{\sqrt{\left(1-\frac{2m_+}{R_0}\right)\left(1-\frac{a_+^2}{R_0^2}\right)}}\right. \\
& \left. +\frac{\left[\frac{m_-}{R_0^2}\left(1-\frac{a_-^2}{R_0^2}\right)+\frac{a_-^2}{R_0^3}\left(1-\frac{2m_-}{R_0}\right)\right]^2}{\left[\left(1-\frac{2m_-}{R_0}\right)\left(1-\frac{a_-^2}{R_0^2}\right)\right]^{3/2}}+\frac{\frac{2m_-}{R_0^3}\left(1-\frac{a_-^2}{R_0^2}\right)+\frac{3a_-^2}{R_0^4}\left(1-\frac{2m_-}{R_0}\right)-\frac{4m_-a_-^2}{R_0^5}}{\sqrt{\left(1-\frac{2m_-}{R_0}\right)\left(1-\frac{a_-^2}{R_0^2}\right)}}\right\}.
\end{aligned}
\tag{50}
$$

More specifically, this last inequality translates the stability condition $V''(R_0) \geq 0$ into an explicit inequality on $m_s''(R_0)$, an inequality that can in particular cases be explicitly checked. In the absence of external forces this inequality is the only stability condition one requires. However, once one has external forces (that is, in the presence of fluxes $\Xi \neq 0$), there is additional information:

$$4\pi R_0^2 \Xi_0 = -\left[\frac{a_+^2}{(R_0^2 - a_+^2)} \sqrt{\left(1 - \frac{2m_+}{R_0}\right)\left(1 - \frac{a_+^2}{R_0^2}\right)} + \frac{a_-^2}{(R_0^2 - a_-^2)} \sqrt{\left(1 - \frac{2m_-}{R_0}\right)\left(1 - \frac{a_-^2}{R_0^2}\right)} \right]. \tag{51}$$

This leads one to consider the quantity

$$[4\pi R_0^2 \Xi_0]' = \frac{a_+^2}{(R_0^2 - a_+^2)} \left[\frac{2R_0}{(R_0^2 - a_+^2)} \sqrt{\left(1 - \frac{2m_+}{R_0}\right)\left(1 - \frac{a_+^2}{R_0^2}\right)} - \frac{\frac{m_+}{R_0^2}\left(1 - \frac{a_+^2}{R_0^2}\right) + \frac{a_+^2}{R_0^3}\left(1 - \frac{2m_+}{R_0}\right)}{\sqrt{\left(1 - \frac{2m_+}{R_0}\right)\left(1 - \frac{a_+^2}{R_0^2}\right)}} \right]$$

$$+ \frac{a_-^2}{(R_0^2 - a_-^2)} \left[\frac{2R_0}{(R_0^2 - a_-^2)} \sqrt{\left(1 - \frac{2m_-}{R_0}\right)\left(1 - \frac{a_-^2}{R_0^2}\right)} - \frac{\frac{m_-}{R_0^2}\left(1 - \frac{a_-^2}{R_0^2}\right) + \frac{a_-^2}{R_0^3}\left(1 - \frac{2m_-}{R_0}\right)}{\sqrt{\left(1 - \frac{2m_-}{R_0}\right)\left(1 - \frac{a_-^2}{R_0^2}\right)}} \right]. \tag{52}$$

Furthermore, note that since $R_0 > a_\pm$, the inequality on $[4\pi R_0^2 \Xi_0]''$ is given by

$$[4\pi R_0^2 \Xi_0]'' \geq \left\{ -\frac{3a_+^2(2R_0^2 + a_+^2)}{(R_0^2 - a_+^2)^3} \sqrt{\left(1 - \frac{2m_+}{R_0}\right)\left(1 - \frac{a_+^2}{R_0^2}\right)} + \frac{4a_+^2 R_0}{(R_0^2 - a_+^2)^2} \frac{\frac{m_+}{R_0^2}\left(1 - \frac{a_+^2}{R_0^2}\right) + \frac{a_+^2}{R_0^3}\left(1 - \frac{2m_+}{R_0}\right)}{\sqrt{\left(1 - \frac{2m_+}{R_0}\right)\left(1 - \frac{a_+^2}{R_0^2}\right)}} \right.$$

$$+ \frac{a_+^2}{(R_0^2 - a_+^2)} \frac{\left[\frac{m_+}{R_0^2}\left(1 - \frac{a_+^2}{R_0^2}\right) + \frac{a_+^2}{R_0^3}\left(1 - \frac{2m_+}{R_0}\right)\right]^2}{\left[\left(1 - \frac{2m_+}{R_0}\right)\left(1 - \frac{a_+^2}{R_0^2}\right)\right]^{3/2}} + \frac{a_+^2}{(R_0^2 - a_+^2)} \frac{\frac{2m_+}{R_0^3}\left(1 - \frac{a_+^2}{R_0^2}\right) + \frac{3a_+^2}{R_0^4}\left(1 - \frac{2m_+}{R_0}\right) - \frac{4m_+ a_+^2}{R_0^5}}{\sqrt{\left(1 - \frac{2m_+}{R_0}\right)\left(1 - \frac{a_+^2}{R_0^2}\right)}} \right\}$$

$$+ \left\{ -\frac{3a_-^2(2R_0^2 + a_-^2)}{(R_0^2 - a_-^2)^3} \sqrt{\left(1 - \frac{2m_-}{R_0}\right)\left(1 - \frac{a_-^2}{R_0^2}\right)} + \frac{4a_-^2 R_0}{(R_0^2 - a_-^2)^2} \frac{\frac{m_-}{R_0^2}\left(1 - \frac{a_-^2}{R_0^2}\right) + \frac{a_-^2}{R_0^3}\left(1 - \frac{2m_-}{R_0}\right)}{\sqrt{\left(1 - \frac{2m_-}{R_0}\right)\left(1 - \frac{a_-^2}{R_0^2}\right)}} \right.$$

$$+ \frac{a_-^2}{(R_0^2 - a_-^2)} \frac{\left[\frac{m_-}{R_0^2}\left(1 - \frac{a_-^2}{R_0^2}\right) + \frac{a_-^2}{R_0^3}\left(1 - \frac{2m_-}{R_0}\right)\right]^2}{\left[\left(1 - \frac{2m_-}{R_0}\right)\left(1 - \frac{a_-^2}{R_0^2}\right)\right]^{3/2}} + \frac{a_-^2}{(R_0^2 - a_-^2)} \frac{\frac{2m_-}{R_0^3}\left(1 - \frac{a_-^2}{R_0^2}\right) + \frac{3a_-^2}{R_0^4}\left(1 - \frac{2m_-}{R_0}\right) - \frac{4m_- a_-^2}{R_0^5}}{\sqrt{\left(1 - \frac{2m_-}{R_0}\right)\left(1 - \frac{a_-^2}{R_0^2}\right)}} \right\}. \tag{53}$$

In summary, the inequalities (50) and (53) dictate the stability regions of the wormhole solutions considered in this work, and in the following section we consider specific applications and examples.

III. APPLICATIONS AND EXAMPLES

In this section, we shall apply the general formalism described above to some specific examples. Several of these special cases are particularly important in order to emphasize the specific features of these black-bounce spacetimes. Some examples are essential to assess the simplifications due to symmetry between the two asymptotic regions, while other cases are useful to understand the

asymmetry between the two universes used in traversable wormhole construction. In the following analysis we will consider specific cases by tuning the parameters of the bulk spacetimes, namely, the bounce parameters $a_\pm$ and the masses $m_\pm$.

A. Vanishing flux term: $a_\pm = 0$

Here, we consider the case of a vanishing flux term, that is, $\Xi = 0$, which is induced by imposing $a_\pm = 0$. Thus, the only stability constraint arises from inequality (50). Note that this case corresponds to the thin-shell Schwarzschild traversable wormholes analyzed in Refs. [25,60]. For the specific case of $a_\pm = 0$, and

considering an asymmetry in the masses $m_- \neq m_+$, inequality (50) reduces to

$$R_0^2 \left[\frac{m_s(R_0)}{R_0} \right]'' \geq F_1(R_0, m_\pm)$$

$$= \frac{\frac{2m_+}{R_0} \left(1 - \frac{3m_+}{2R_0} \right)}{\left(1 - \frac{2m_+}{R_0} \right)^{3/2}} + \frac{\frac{2m_-}{R_0} \left(1 - \frac{3m_-}{2R_0} \right)}{\left(1 - \frac{2m_-}{R_0} \right)^{3/2}}. \quad (54)$$

Note that in order to plot the stability regions, we have defined the following dimensionless form of the constraint as $F_1(R_0, m_\pm) = R_0^2 [m_s(R_0)/R_0]''$, which is depicted as the surfaces given in the plots of Fig. 1. The stability regions lie above these surfaces. To visualize the whole range of the parameters, so as to bring infinite R_0 in to a finite region of the plot, we have considered the definition $x = 2m_+/R_0$ for convenience. For instance, the limit $R_0 \to \infty$ corresponds to $x \to 0$, and $R_0 = 2m_+$ is equivalent to $x = 1$. Thus, we have considered the range $0 < x < 1$.

In the left plot of Fig. 1, we have considered the parameter $y_1 = m_-/m_+$, which lies within the range $0 < y_1 < 1/x$. This parameter provides information on the relative variation of the masses. However, one may also consider a more symmetrical form of the stability analysis, by considering the definition $y_2 = 2m_-/R_0$, which possesses the range $0 < y_2 < 1$, and the stability

region is depicted in the right plot of Fig. 1. These two plots provide complementary information.

Regarding the stability of the solution, from Fig. 1 we verify that large stability regions exist for low values of $x = 2m_+/R_0$ and of $y_1 = m_-/m_+$ (and of $y_2 = 2m_-/R_0$). For regions close to the event horizon, $x \to 1$, the stability region decreases in size and only exists for low values of $y_{1,2}$. The specific case of $y_1 = m_-/m_+ = 1$ corresponds to the thin-shell Schwarzschild wormholes analyzed in [60], and one verifies that the size of the stability regions increases as the junction interface of the thin-shell increases, namely, as $x = 2m_+/R_0 \to 0$, as is transparent from Fig. 1.

B. Vanishing mass: $a_+ \neq a_-$ and $m_\pm = 0$

Consider now the case of vanishing mass terms $m_\pm = 0$, with an asymmetry of the bounce parameters $a_+ \neq a_-$. For this case, inequality (50) reduces to

$$R_0^2 \left[\frac{m_s(R_0)}{R_0} \right]'' \geq F_2(R_0, a_\pm)$$

$$= 2 \left[\frac{\frac{a_+^2}{R_0^2} \left(\frac{3}{2} - \frac{a_+^2}{R_0^2} \right)}{\left(1 - \frac{a_+^2}{R_0^2} \right)^{3/2}} + \frac{\frac{a_-^2}{R_0^2} \left(\frac{3}{2} - \frac{a_-^2}{R_0^2} \right)}{\left(1 - \frac{a_-^2}{R_0^2} \right)^{3/2}} \right], \quad (55)$$

and inequality (53) takes the following form:
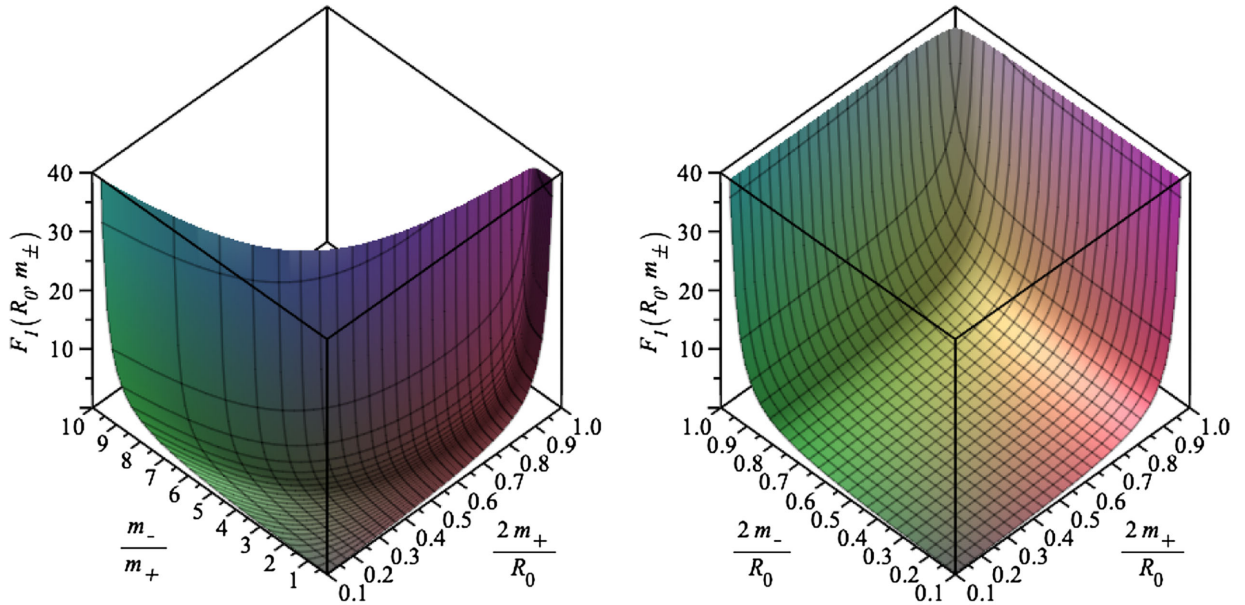

FIG. 1. Stability analysis for thin-shell Schwarzschild traversable wormholes, taking into account that $a_\pm = 0$ and $m_- \neq m_+$. The surfaces are given by the dimensionless quantity $F_1(R_0, m_\pm)$, defined by the right-hand side of inequality (54). The stability regions lie above the surfaces depicted in the plots. We have considered the range $0 < x = 2m_+/R_0 < 1$ and $0 < y_1 = m_-/m_+ < 1/x$ in the left plot and $0 < y_2 = 2m_-/R_0 < 1$ in the right plot, respectively. Note that large stability regions exist for low values of $x = 2m_+/R_0$ and of $y_{1,2}$. For regions close to the event horizon, $x \to 1$, the stability region decreases in size and only increases significantly for low values of y_1. See the text for details.

$$R_0^2[4\pi R_0^2 \Xi(R_0)]'' \geq G_2(R_0, a_\pm)$$

$$= -\frac{\frac{a_+^2}{R_0^2}\left(6 - 4\frac{a_+^2}{R_0^2} + 2\frac{a_+^4}{R_0^4}\right)}{\left(1 - \frac{a_+^2}{R_0^2}\right)^{5/2}}$$

$$- \frac{\frac{a_-^2}{R_0^2}\left(6 - 4\frac{a_-^2}{R_0^2} + 2\frac{a_-^4}{R_0^4}\right)}{\left(1 - \frac{a_-^2}{R_0^2}\right)^{5/2}}. \qquad (56)$$

We now consider the definition of the parameters $x = a_+/R_0$ and $y = a_-/R_0$ for convenience, so as to bring infinite R_0 within a finite region of the plot. That is, $R_0 \to \infty$ is represented as $x \to 0$; and $R_0 = a_+, a_-$ is equivalent to x, $y = 1$. Thus, the parameters x and y are restricted to the ranges $0 < x < 1$ and $0 < y < 1$. Inequality (55) is depicted as the upper surface in Fig. 2 and inequality (56) is depicted as the lower surface; the stability regions are given above the respective surfaces. Thus, the final stability region lies above the upper surface.

C. Asymmetric vanishing parameters: $a_+ = 0$ and $m_- = 0$

Consider now the case of vanishing interior mass $m_- = 0$, and vanishing exterior parameter $a_+ = 0$. For this case, the inequality (50) reduces to

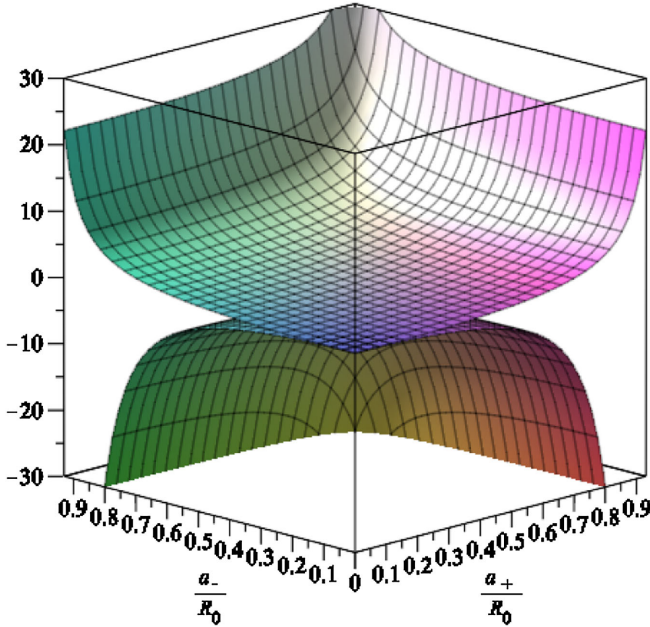$$R_0^2\left[\frac{m_s(R_0)}{R_0}\right]'' \geq F_3(R_0, m_+, a_-)$$

$$= \left[\frac{\frac{2m_+}{R_0}\left(1 - \frac{3m_+}{2R_0}\right)}{\left(1 - \frac{2m_+}{R_0}\right)^{3/2}} + \frac{\frac{3a_-^2}{R_0^2}\left(1 - \frac{2a_-^2}{3R_0^2}\right)}{\left(1 - \frac{a_-^2}{R_0^2}\right)^{3/2}}\right], \qquad (57)$$

and inequality (53) is given by

$$R_0^2[4\pi R_0^2 \Xi(R_0)]'' \geq G_3(R_0, a_-) = -\frac{2\frac{a_-^2}{R_0^2}\left(3 - 2\frac{a_-^2}{R_0^2} + \frac{a_-^4}{R_0^4}\right)}{\left(1 - \frac{a_-^2}{R_0^2}\right)^{5/2}}. \qquad (58)$$

These are depicted as the upper and lower surfaces, respectively, in Fig. 3. As in the previous example, the final stability region of the solution lies above the upper surface.

D. Mirror symmetry: $a_\pm = a$ and $m_\pm = m$

Consider, for simplicity, the symmetric case, i.e., $a_\pm = a$ and $m_\pm = m$, so that the stability conditions reduce to

FIG. 2. The upper surface depicts the quantity $F_2(R_0, a_\pm) = R_0^2[m_s(R_0)/R_0]''$, and the stable region lies above the surface of that curve. On the other hand, the function $G_2(R_0, a_\pm) = R_0^2[4\pi R_0^2\Xi_0]''$ is depicted by the lower surface, and the stable region also lies above the surface of that curve. Thus the final stability region of the solution lies above the upper surface. See the text for more details.
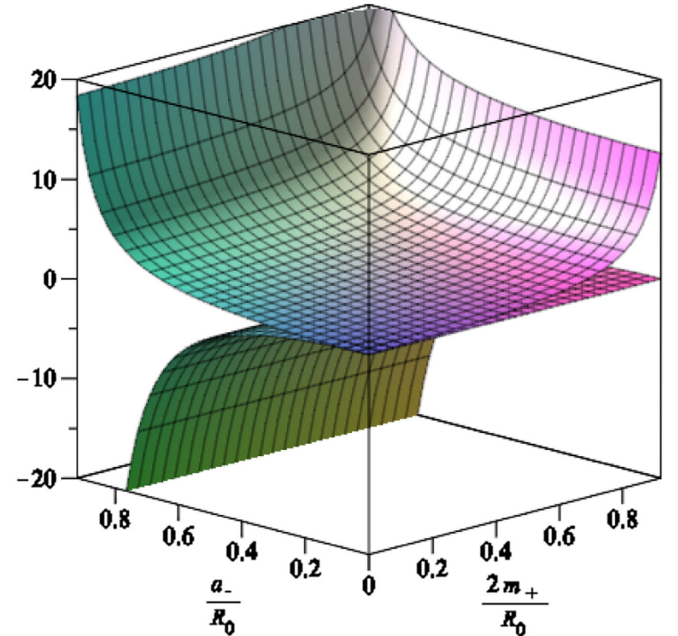
FIG. 3. The upper surface depicts the quantity $F_3(R_0, m_+, a_-) = R_0^2[m_s(R_0)/R_0]''$, and the stable region lies above that surface. On the other hand, the function $G_3(R_0, a_-) = R_0^2[4\pi R_0^2\Xi_0]''$ is depicted by the lower surface, and the stable region also lies above that surface of that plot. Thus, the final stability region of the solution lies above the upper surface. See the text for more details.

$$R_0^2 \left[\frac{m_s(R_0)}{R_0}\right]'' \geq 2 \left\{ \frac{\left[\frac{m}{R_0}\left(1 - \frac{a^2}{R_0^2}\right) + \frac{a^2}{R_0^2}\left(1 - \frac{2m}{R_0}\right)\right]^2}{\left[\left(1 - \frac{2m}{R_0}\right)\left(1 - \frac{a^2}{R_0^2}\right)\right]^{3/2}} + \frac{\frac{2m}{R_0}\left(1 - \frac{a^2}{R_0^2}\right) + \frac{3a^2}{R_0^2}\left(1 - \frac{2m}{R_0}\right) - \frac{4ma^2}{R_0^3}}{\sqrt{\left(1 - \frac{2m}{R_0}\right)\left(1 - \frac{a^2}{R_0^2}\right)}} \right\} \tag{59}$$

and

$$R_0^2 [4\pi R_0^2 \Xi_0]'' \geq \frac{2a^2}{(R_0^2 - a^2)} \left\{ -\frac{3R_0^2(2R_0^2 + a^2)}{(R_0^2 - a^2)^2}\sqrt{\left(1 - \frac{2m}{R_0}\right)\left(1 - \frac{a^2}{R_0^2}\right)} + \frac{4R_0^2}{(R_0^2 - a^2)} \frac{\frac{m}{R_0}\left(1 - \frac{a^2}{R_0^2}\right) + \frac{a^2}{R_0^2}\left(1 - \frac{2m}{R_0}\right)}{\sqrt{\left(1 - \frac{2m}{R_0}\right)\left(1 - \frac{a^2}{R_0^2}\right)}} \right.$$

$$\left. + \frac{\left[\frac{m}{R_0}\left(1 - \frac{a^2}{R_0^2}\right) + \frac{a^2}{R_0^2}\left(1 - \frac{2m}{R_0}\right)\right]^2}{\left[\left(1 - \frac{2m}{R_0}\right)\left(1 - \frac{a^2}{R_0^2}\right)\right]^{3/2}} + \frac{\frac{2m}{R_0}\left(1 - \frac{a^2}{R_0^2}\right) + \frac{3a^2}{R_0^2}\left(1 - \frac{2m}{R_0}\right) - \frac{4ma^2}{R_0^3}}{\sqrt{\left(1 - \frac{2m}{R_0}\right)\left(1 - \frac{a^2}{R_0^2}\right)}} \right\}, \tag{60}$$

respectively.

It is useful to express inequality (59) in the following dimensionless form $F_4(R_0, m, a) = R_0^2[m_s(R_0)/R_0]''$ and inequality (60) as $G_4(R_0, m, a) = R_0^2[4\pi R_0^2 \Xi_0]''$. Both surfaces are depicted in Fig. 4, and the final stability region is situated above the intersection of the surfaces.
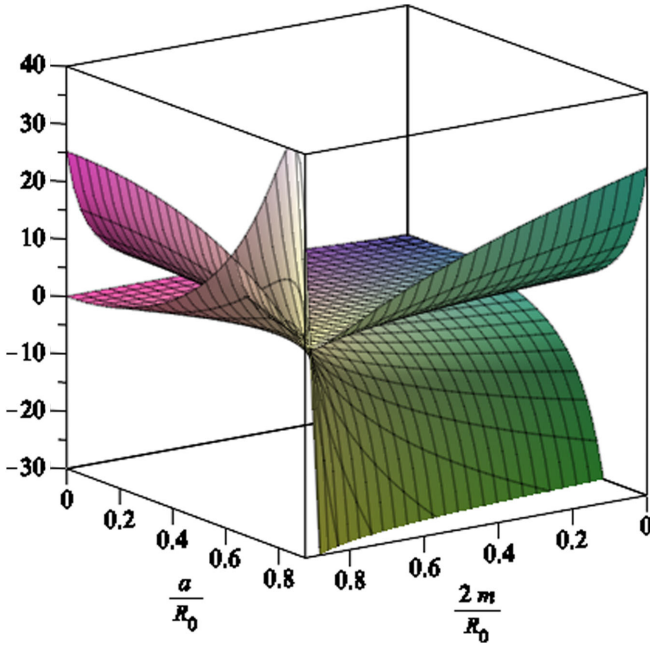

FIG. 4. The upper surface depicts the quantity $F_4(R_0, m, a) = R_0^2[m_s(R_0)/R_0]''$, and the stable region lies above that surface. On the other hand, the function $G_4(R_0, m, a) = R_0^2[4\pi R_0^2 \Xi_0]''$ is depicted by the lower surface, and the stable region also lies above that surface. The final stability region of the solution lies above the intersection of both surfaces. Note that inequality (60) serves to decrease the stability region for high values of x and y. See the text for more details.

Note that we have considered the definition $x = 2m/R_0$ for convenience, so as to bring infinite R_0 within a finite region of the plot. That is, $R_0 \to \infty$ is represented as $x \to 0$, and $R_0 = 2m$ is equivalent to $x = 1$. Thus, the parameter x is restricted to the range $0 < x < 1$. We also define the parameter $y = a/R_0$, which also lies in the range $0 < y < 1$. It is interesting to note that the inequality (60) serves to decrease the stability region for high values of x and y, as is transparent from Fig. 4.

E. Two specific asymmetric cases

1. $a_+ \neq a_-$ and $m_+ = m_-$

Consider the case of symmetric masses $m_\pm = m$, but with asymmetric bounce parameters $a_+ \neq a_-$. To analyze the stability regions we define $a_+ = \alpha a_-$, where $\alpha \in \Re^+$. Rather than write down the explicit form of the inequalities which are rather lengthy and messy, we present the dimensionless form of inequalities (50) and (53) as the upper and lower surfaces in the plots of Figs. 5 and 6. Note that the specific case of $\alpha = 1$ reduces to the analysis of the mirror symmetry considered in the previous Sec. III D. We consider the dimensionless parameters $x = 2m/R_0$ and $y = a_-/R_0$ in order to analyze the stability regions. In the following we separate the cases $\alpha < 1$ and $\alpha > 1$.

(i) *Specific case of $\alpha < 1$:* the upper and lower surfaces in Fig. 5 depict the functions $F_5(R_0, m, a_\pm) = R_0^2[m_s(R_0)/R_0]''$ and $G_5(R_0, m, a_\pm) = R_0^2[4\pi R_0^2 \Xi_0]''$, respectively, and the stability regions representing the inequalities (50) and (53) are the regions above these surfaces. The range of the dimensionless parameters is $0 < x, y < 1$. We have considered $\alpha = 0.9$ in the left plot and $\alpha = 0.4$ in the right plot of Fig. 5. As the final stability region of the solution lies above the intersection of both surfaces, we note
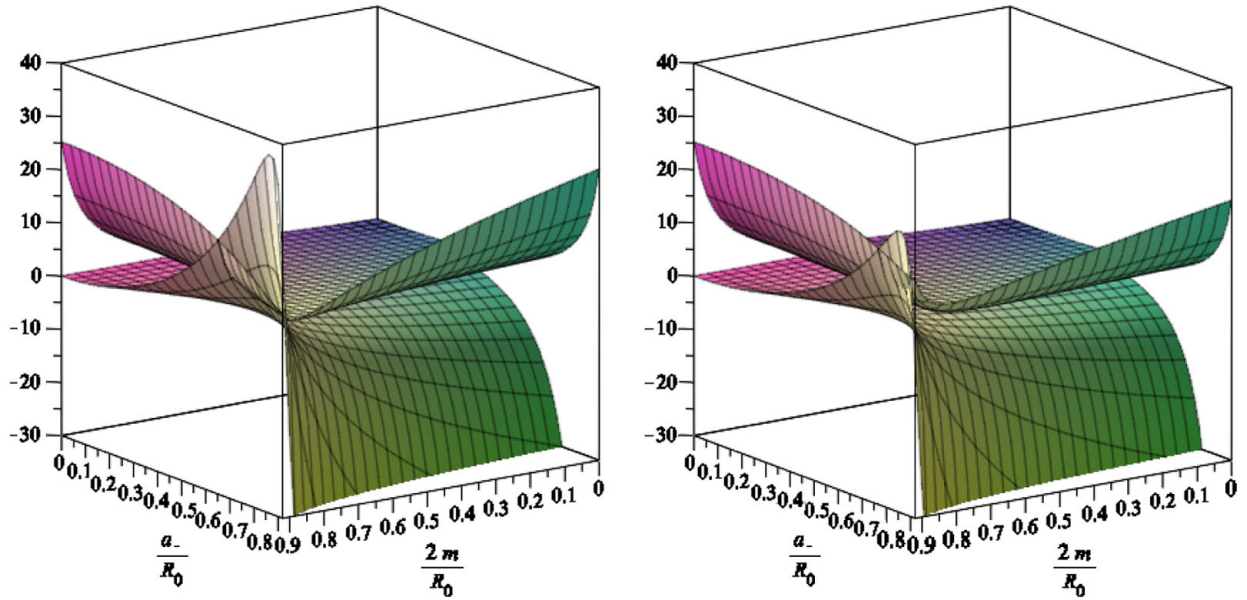
FIG. 5. Specific case of $a_+ = \alpha a_-$ and $m_+ = m_-$ for $\alpha < 1$: The upper surface depicts the quantity $F_5(R_0, m, a_\pm) = R_0^2[m_s(R_0)/R_0]''$, and the function $G_5(R_0, m, a_\pm) = R_0^2[4\pi R_0^2 \Xi_0]''$ is depicted by the lower surface. The stable regions are given above the surfaces. We have considered $\alpha = 0.9$ in the left plot and $\alpha = 0.4$ in the right plot. Note that decreasing the value of α serves to decrease the lower surface representing inequality (53), and thus increase the final stability region. See the text for more details.

that decreasing the value of α qualitatively serves to decrease the lower surface representing inequality (53), and thus increase the final stability region. This is transparent for high values of x and y.

(ii) *Specific case of $\alpha > 1$:* the analysis is analogous to the above case and is depicted in Fig. 6; however, here the left plot is given by $\alpha = 1.5$ and the right plot by $\alpha = 3$. The range of the dimensionless
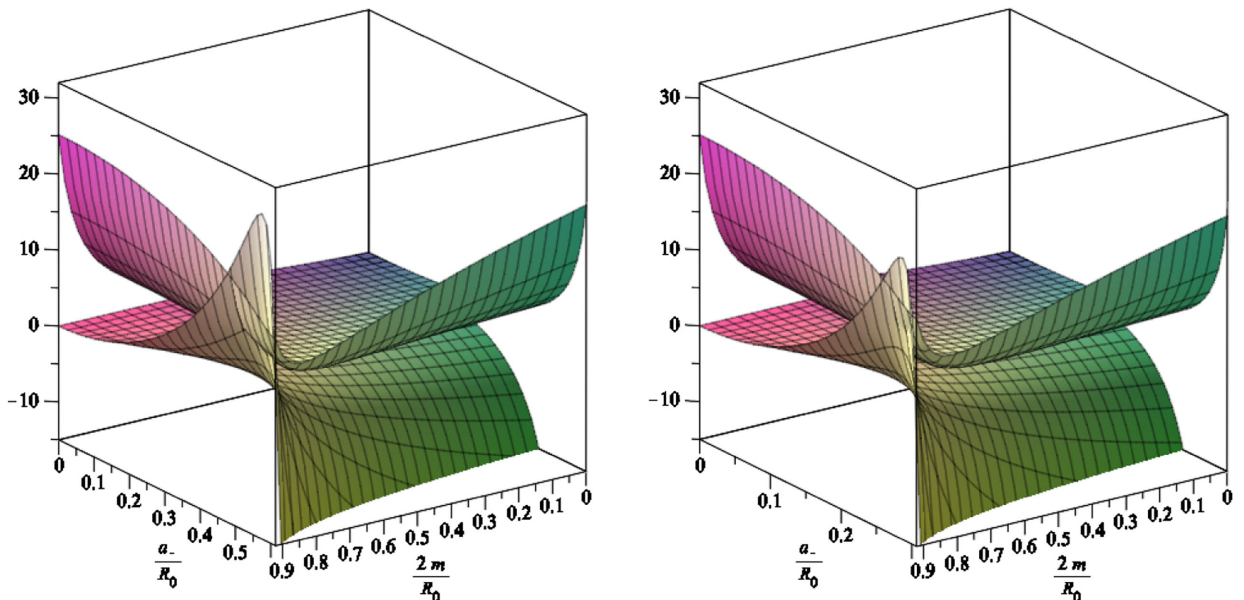

FIG. 6. Specific case of $a_+ = \alpha a_-$ and $m_+ = m_-$ for $\alpha > 1$: The upper and lower surfaces depict the quantities $F_5(R_0, m, a_\pm) = R_0^2[m_s(R_0)/R_0]''$ and $G_5(R_0, m, a_\pm) = R_0^2[4\pi R_0^2 \Xi_0]''$, respectively. The stable regions are given above the surfaces. We have considered $\alpha = 1.5$ in the left plot and $\alpha = 3$ in the right plot. Note that increasing the value of α, serves to decrease the lower surface representing inequality (60), and thus increase the final stability region. However, the range for y decreases for increasing values of α (for $\alpha = 1.5$, the range is $0 < y < 2/3$, and for $\alpha = 3$, it is $0 < y < 1/3$). See the text for more details.
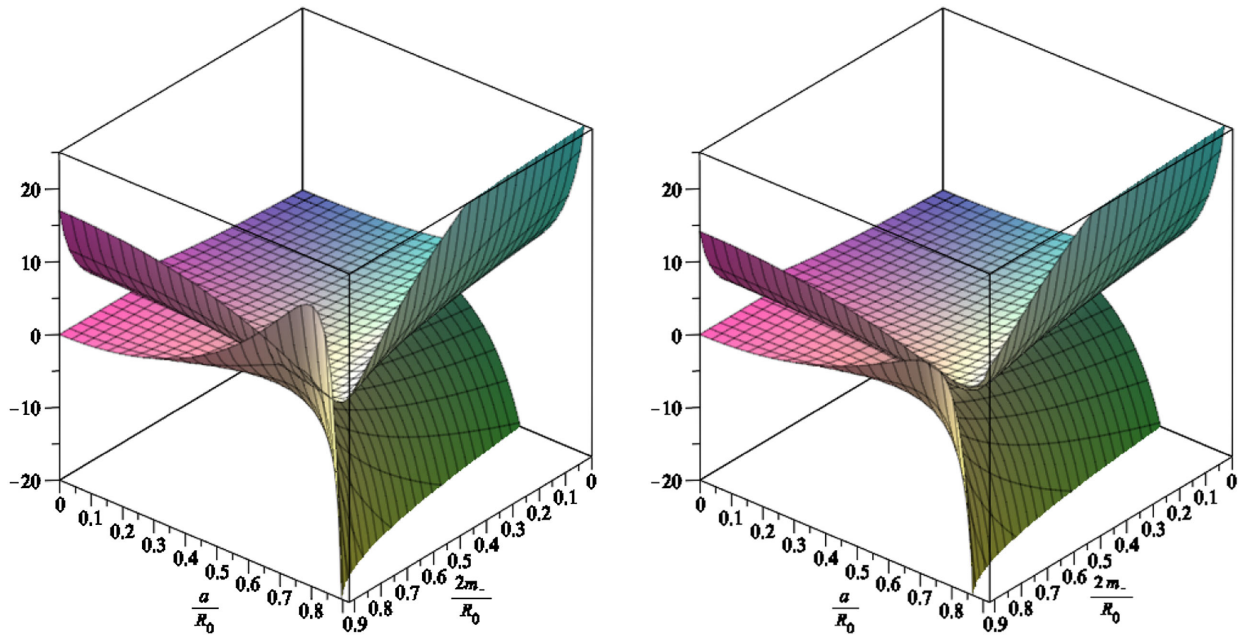
FIG. 7.   Specific case of $a_+ = a_-$ and $m_+ = \alpha m_-$ for $\alpha < 1$. We consider the dimensionless parameters $x = 2m_-/R_0$ and $y = a/R_0$. We have considered $\alpha = 0.9$ in the left plot and $\alpha = 0.7$ in the right plot. Note that decreasing the value of α serves to decrease the lower surface representing inequality (53), and thus increase the final stability region. See the text for more details.

parameters is given by $0 < x < 1$ and $0 < y < 1/\alpha$. As in the previous example, the final stability region of the solution lies above the intersection of both surfaces depicted in Fig. 6. Note that increasing the value of α serves to decrease the lower surface representing inequality (53),

and thus increase the final stability region. However, the range for y decreases for increasing values of α (for $\alpha = 1.5$, the range is $0 < y < 2/3$, and for $\alpha = 3$, it is $0 < y < 1/3$). This analysis is transparent for high values of x and y in Fig. 6.
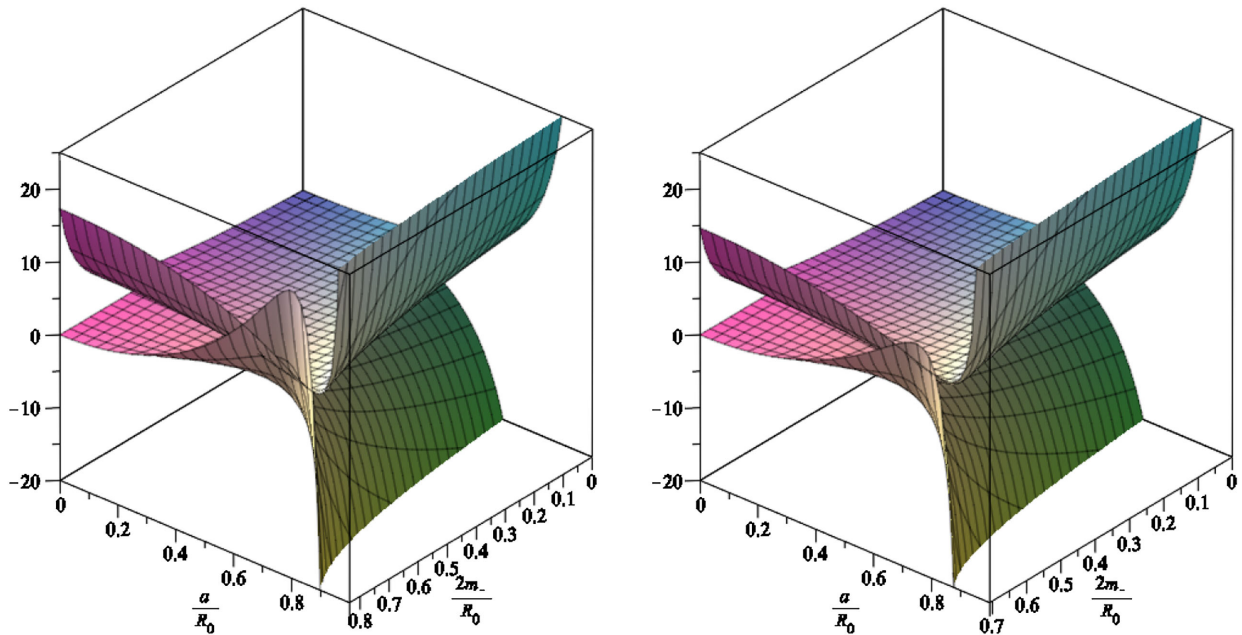

FIG. 8.   Specific case of $a_+ = a_-$ and $m_+ = \alpha m_-$ for $\alpha > 1$. We consider the dimensionless parameters $x = 2m_-/R_0$ and $y = a/R_0$. We have considered $\alpha = 1.1$ in the left plot and $\alpha = 1.3$ in the right plot. Note that increasing the value of α serves to decrease the lower surface representing inequality (53), and thus increase the final stability region. See the text for more details.

2. $a_+ = a_-$ and $m_+ \neq m_-$

Here we consider the case of asymmetric masses $m_\pm \neq m$, but with symmetric bounce parameters $a_\pm = a$, and for simplicity define $m_+ = \alpha m_-$, where $\alpha \in \Re^+$. As in the specific case previously given above, we present the dimensionless form of inequalities (50) and (53) as the upper and lower surfaces in the plots of Figs. 7 and 8. We consider the dimensionless parameters $x = 2m_-/R_0$ and $y = a/R_0$, in order to analyze the stability regions, and as in the previous example we separate the cases $\alpha < 1$ and $\alpha > 1$.

(i) *Specific case of $\alpha < 1$*: the functions $F_6(R_0, m, a_\pm) = R_0^2[m_s(R_0)/R_0]''$ and $G_6(R_0, m, a_\pm) = R_0^2[4\pi R_0^2 \Xi_0]''$ are depicted by the upper and lower surfaces in Fig. 7, respectively, and the stability regions representing the inequalities (50) and (53) are given above these surfaces. The range of the dimensionless parameters is $0 < x, y < 1$. We have considered $\alpha = 0.9$ in the left plot and $\alpha = 0.7$ in the right plot of Fig. 7. The final stability region of the solution lies above the intersection of both surfaces. Note that decreasing the value of α serves to decrease the lower surface representing inequality (53), and thus increase the final stability region.

(ii) *Specific case of $\alpha > 1$*: analogous to the above case, the stability regions are depicted in Fig. 8. The left plot is given by $\alpha = 1.1$ and the right plot by $\alpha = 1.3$. The range of the dimensionless parameters is given by $0 < x < 1$ and $0 < y < 1/\alpha$. As in the previous example, the final stability region of the solution lies above the intersection of both surfaces depicted in Fig. 8. Note that increasing the value of α serves to decrease the lower surface representing inequality (53), and thus increase the final stability region. However, the range for y decreases for increasing values of α.

IV. CONCLUSION

In this article we have considered thin-shell wormholes based on the recently introduced black-bounce spacetimes. Specifically, by matching two black-bounce spherically symmetric spacetimes using the cut-and-paste procedure, we have analyzed the stability and evolution of dynamic thin-shell black-bounce wormholes. We have explored the parameter space of various models depending on the bulk masses $m_\pm$, and the values of the bulk bounce parameter $a_\pm$, investigating the internal dynamics of the thin-shell connecting the two bulk spacetimes, and demonstrating the existence of suitable stability regions in parameter space. Several of these models are particularly useful in order to emphasize the specific features of these black-bounce spacetimes. For instance, some examples are important to assess the simplifications due to symmetry between the two asymptotic regions, while other cases are useful to understand the asymmetry between the two universes used in traversable wormhole construction. Indeed, the interesting physics is encoded in the parameter $a_\pm$ which characterizes the scale of the bounce, and that emphasizes the features of these spacetimes. In fact, the presence of the parameter $a_\pm$ induces the flux term in the conservation identity, which is responsible for the net discontinuity in the bulk momentum flux which impinges on the shell. Thus, due to this flux term, the bounce parameter places an additional constraint on the stability analysis of the spacetime geometry.

From the linearized stability analysis one may assess and understand the (a)symmetry between the two universes in the traversable wormhole construction. For instance, consider the simple case of vanishing mass $m_\pm = 0$ and $a_\pm \neq 0$ analyzed in Sec. III B, where large stability regions exist for $a_\pm \ll R_0$. However, the low stability region for the specific case of $a_+ \sim R_0$, increases significantly for the asymmetric case of decreasing the value of a_-. Another interesting example is the asymmetric case analyzed in Sec. III C, where we considered $a_+ = 0$ and $m_- = 0$. Here, the low stability regions for $a_- \sim R_0$ and $m_+ \sim R_0$ may be significantly increased by decreasing the asymmetric parameters, until large stability regions are present for $a_- \ll R_0$ and $m_+ \ll R_0$. The mirror symmetric case of $a_\pm = a$ and $m_\pm = m$ considered in Sec. III D is of particular interest. Despite the fact that large stability regions exist for $a \ll R_0$ and $m \ll R_0$, the region at $a \approx R_0$ and $m \approx R_0$ is of particular interest. Here the flux term constraint kicks in and lowers the stability region significantly. In fact, analyzing this specific region for the asymmetric case is particularly interesting, as one may explore the asymmetry between the universes in the wormhole construction by considering the case of $a_+ \neq a_-$ in Sec. III E. More specifically, by varying the relative values of a_+ and a_-, the analysis showed that one could increase or decrease the stability regions, and one may assess and understand the (a)symmetry between the two universes in the traversable wormhole construction. In concluding, the constructions considered in this work are sufficiently novel to be interesting, and sufficiently straightforward to be tractable.

[1] L. Flamm, Beitrage zur Einsteinschen Gravitationstheorie, Phys. Z. **17**, 448 (1916).

[2] A. Einstein and N. Rosen, The particle problem in the General Theory of Relativity, Phys. Rev. **48**, 73 (1935).

[3] J. A. Wheeler, Geons, Phys. Rev. **97**, 511 (1955).

[4] H. G. Ellis, Ether flow through a drainhole: A particle model in general relativity, J. Math. Phys. (N.Y.) **14**, 104 (1973).

[5] H. G. Ellis, The evolving, flowless drain hole: A non-gravitating particle model in general relativity theory, Gen. Relativ. Gravit. **10**, 105 (1979).

[6] K. A. Bronnikov, Scalar-tensor theory and scalar charge, Acta Phys. Pol. B **4**, 251 (1973).

[7] G. Clement, Axisymmetric regular multiwormhole solutions in five-dimensional general relativity, Gen. Relativ. Gravit. **16**, 477 (1984).

[8] M. Morris and K. S. Thorne, Wormholes in spacetime and their use for interstellar travel: A tool for teaching General Relativity, Am. J. Phys. **56**, 395 (1988).

[9] M. S. Morris, K. S. Thorne, and U. Yurtsever, Wormholes, Time Machines, and the Weak Energy Condition, Phys. Rev. Lett. **61**, 1446 (1988).

[10] M. Visser, Traversable wormholes from surgically modified Schwarzschild space-times, Nucl. Phys. **B328**, 203 (1989).

[11] M. Visser, Traversable wormholes: Some simple examples, Phys. Rev. D **39**, 3182 (1989).

[12] M. Visser, Wormholes, baby universes and causality, Phys. Rev. D **41**, 1116 (1990).

[13] M. Visser, Quantum mechanical stabilization of minkowski signature wormholes, Phys. Lett. B **242**, 24 (1990).

[14] M. Visser, Wormholes and interstellar travel, Los Alamos Scientific Laboratory, Report No. LA-UR-89-1008.

[15] M. Visser, Quantum wormholes in Lorentzian signature, in *Proceedings of the 1990 DPF Conference, Rice University, Houston* (World Scientific, Singapore, 1990), pp. 0858–0860.

[16] D. Hochberg, Lorentzian wormholes in higher order gravity theories, Phys. Lett. B **251**, 349 (1990).

[17] V. P. Frolov and I. D. Novikov, Physical effects in wormholes and time machine, Phys. Rev. D **42**, 1057 (1990).

[18] M. Visser, Quantum wormholes, Phys. Rev. D **43**, 402 (1991).

[19] M. Visser, Wheeler wormholes and topology change, Mod. Phys. Lett. A **06**, 2663 (1991).

[20] M. Visser, From wormhole to time machine: Comments on Hawking's chronology protection conjecture, Phys. Rev. D **47**, 554 (1993).

[21] M. Visser, van Vleck determinants: Traversable wormhole space-time, Phys. Rev. D **49**, 3963 (1994).

[22] J. G. Cramer, R. L. Forward, M. S. Morris, M. Visser, G. Benford, and G. A. Landis, Natural wormholes as gravitational lenses, Phys. Rev. D **51**, 3117 (1995).

[23] S. Kar, Evolving wormholes and the weak energy condition, Phys. Rev. D **49**, 862 (1994).

[24] S. Kar and D. Sahdev, Evolving Lorentzian wormholes, Phys. Rev. D **53**, 722 (1996).

[25] E. Poisson and M. Visser, Thin shell wormholes: Linearization stability, Phys. Rev. D **52**, 7318 (1995).

[26] M. Visser, *Lorentzian Wormholes: From Einstein to Hawking* (AIP Press [now Springer], New York, 1995).

[27] D. Hochberg and M. Visser, Geometric structure of the generic static traversable wormhole throat, Phys. Rev. D **56**, 4745 (1997).

[28] M. Visser and D. Hochberg, Generic wormhole throats, Ann. Isr. Phys. Soc. **13**, 249 (1997).

[29] M. Visser, Traversable wormholes: The Roman ring, Phys. Rev. D **55**, 5212 (1997).

[30] E. Teo, Rotating traversable wormholes, Phys. Rev. D **58**, 024014 (1998).

[31] D. Hochberg and M. Visser, Null Energy Condition in Dynamic Wormholes, Phys. Rev. Lett. **81**, 746 (1998).

[32] D. Hochberg and M. Visser, Dynamic wormholes, anti-trapped surfaces, and energy conditions, Phys. Rev. D **58**, 044021 (1998).

[33] D. Hochberg and M. Visser, General dynamic wormholes and violation of the null energy condition, arXiv:gr-qc/9901020.

[34] D. Hochberg, C. Molina-París, and M. Visser, Tolman wormholes violate the strong energy condition, Phys. Rev. D **59**, 044011 (1999).

[35] C. Barceló and M. Visser, Traversable wormholes from massless conformally coupled scalar fields, Phys. Lett. B **466**, 127 (1999).

[36] M. Visser, Gravitational vacuum polarization. 1: Energy conditions in the Hartle–Hawking vacuum, Phys. Rev. D **54**, 5103 (1996).

[37] M. Visser, Gravitational vacuum polarization. 2: Energy conditions in the Boulware vacuum, Phys. Rev. D **54**, 5116 (1996).

[38] M. Visser, Gravitational vacuum polarization. 3: Energy conditions in the $(1 + 1)$ Schwarzschild space-time, Phys. Rev. D **54**, 5123 (1996).

[39] M. Visser, Gravitational vacuum polarization. 4: Energy conditions in the Unruh vacuum, Phys. Rev. D **56**, 936 (1997).

[40] M. Visser, Gravitational vacuum polarization, arXiv:gr-qc/9710034.

[41] M. Visser and C. Barceló, *Energy conditions and their cosmological implications, Proceedings of the COSMO99 conference* (World Scientific Publishing, Singapore, 2000).

[42] P. Martín-Moruno and M. Visser, Classical and semiclassical energy conditions, Fundam. Theor. Phys. **189**, 193 (2017), (formerly Lecture Notes in Physics).

[43] C. Barceló and M. Visser, Brane surgery: Energy conditions, traversable wormholes, and voids, Nucl. Phys. **B584**, 415 (2000).

[44] C. Barceló and M. Visser, Scalar fields, energy conditions, and traversable wormholes, Classical Quantum Gravity **17**, 3843 (2000).

[45] N. Dadhich, S. Kar, S. Mukherji, and M. Visser, $R = 0$ space-times and selfdual Lorentzian wormholes, Phys. Rev. D **65**, 064004 (2002).

[46] C. Barceló and M. Visser, Twilight for the energy conditions?, Int. J. Mod. Phys. D **11**, 1553 (2002).

[47] M. Visser, S. Kar, and N. Dadhich, Traversable Wormholes with Arbitrarily Small Energy Condition Violations, Phys. Rev. Lett. **90**, 201102 (2003).

[48] S. Kar, N. Dadhich, and M. Visser, Quantifying energy condition violations in traversable wormholes, Pramana **63,** 859 (2004).

[49] F. S. N. Lobo and M. Visser, Fundamental limitations on 'warp drive' spacetimes, Classical Quantum Gravity **21,** 5871 (2004).

[50] A. V. B. Arellano and F. S. N. Lobo, Evolving wormhole geometries within nonlinear electrodynamics, Classical Quantum Gravity **23,** 5811 (2006).

[51] F. S. N. Lobo, A General class of braneworld wormholes, Phys. Rev. D **75,** 064027 (2007).

[52] F. S. N. Lobo, Exotic solutions in General Relativity: Traversable wormholes and 'warp drive' spacetimes, Classical Quantum Gravity Research (Nova Science Publishers, New York, 2008), pp. 1–78, ISBN 978-1-60456-366-5.

[53] C. G. Boehmer, T. Harko, and F. S. N. Lobo, Conformally symmetric traversable wormholes, Phys. Rev. D **76,** 084014 (2007).

[54] C. G. Boehmer, T. Harko, and F. S. N. Lobo, Wormhole geometries with conformal motions, Classical Quantum Gravity **25,** 075016 (2008).

[55] F. S. N. Lobo, General class of wormhole geometries in conformal Weyl gravity, Classical Quantum Gravity **25,** 175006 (2008).

[56] F. S. N. Lobo and M. A. Oliveira, Wormhole geometries in $f(R)$ modified theories of gravity, Phys. Rev. D **80,** 104012 (2009).

[57] N. Montelongo-García and F. S. N. Lobo, Wormhole geometries supported by a nonminimal curvature-matter coupling, Phys. Rev. D **82,** 104018 (2010).

[58] N. Montelongo-García and F. S. N. Lobo, Nonminimal curvature-matter coupled wormholes with matter satisfying the null energy condition, Classical Quantum Gravity **28,** 085018 (2011).

[59] C. G. Boehmer, T. Harko, and F. S. N. Lobo, Wormhole geometries in modified teleparallel gravity and the energy conditions, Phys. Rev. D **85,** 044033 (2012).

[60] N. Montelongo-García, F. S. N. Lobo, and M. Visser, Generic spherically symmetric dynamic thin-shell traversable wormholes in standard general relativity, Phys. Rev. D **86,** 044026 (2012).

[61] F. S. N. Lobo, P. Martín-Moruno, N. Montelongo-García, and M. Visser, Linearised stability analysis of generic thin shells, arXiv:1211.0605.

[62] T. Harko, F. S. N. Lobo, M. K. Mak, and S. V. Sushkov, Modified-gravity wormholes without exotic matter, Phys. Rev. D **87,** 067504 (2013).

[63] M. R. Mehdizadeh, M. Kord Zangeneh, and F. S. N. Lob0, Einstein-Gauss-Bonnet traversable wormholes satisfying the weak energy condition, Phys. Rev. D **91,** 084004 (2015).

[64] M. Kord Zangeneh, F. S. N. Lobo, and M. H. Dehghani, Traversable wormholes satisfying the weak energy condition in third-order Lovelock gravity, Phys. Rev. D **92,** 124049 (2015).

[65] F. S. N. Lobo, M. Bouhmadi-López, P. Martín-Moruno, N. Montelongo-García, and M. Visser, A novel approach to thin-shell wormholes and applications, arXiv:1512.08474.

[66] P. Boonserm, T. Ngampitipan, A. Simpson, and M. Visser, Exponential metric represents a traversable wormhole, Phys. Rev. D **98,** 084048 (2018).

[67] A. Simpson and M. Visser, Black-bounce to traversable wormhole, J. Cosmol. Astropart. Phys. 02 (2019) 042.

[68] A. Simpson, P. Martín-Moruno, and M. Visser, Vaidya spacetimes, black-bounces, and traversable wormholes, Classical Quantum Gravity **36,** 145007 (2019).

[69] F. S. N. Lobo, Wormholes, warp drives and energy conditions, Fundam. Theor. Phys. **189** (2017).

[70] J. L. Rosa, J. P. S. Lemos, and F. S. N. Lobo, Wormholes in generalized hybrid metric-Palatini gravity obeying the matter null energy condition everywhere, Phys. Rev. D **98,** 064054 (2018).

[71] N. Sen, Über die grenzbedingungen des schwerefeldes an unsteig keitsflächen, Ann. Phys. (Leipzig) **73,** 365 (1924).

[72] K. Lanczos, Flächenhafte verteiliung der materie in der Einsteinschen gravitationstheorie, Ann. Phys. (Leipzig) **74,** 518 (1924).

[73] G. Darmois, Mémorial des sciences mathématiques XXV, Fascicule XXV ch V (Gauthier-Villars, Paris, France, 1927).

[74] J. L.. O'Brien and S. Synge, Jump conditions at discontinuities in general relativity, Commun. Dublin Inst. Adv. Stud. A **9** (1952), https://www.stp.dias.ie/Communications/DIAS-STP-Communications-009-OBrienandSynge.pdf.

[75] A. Lichnerowicz, Théories Relativistes de la Gravitation et de l'Electromagnetisme, Masson, Paris (Masson et C. Editeurs, Paris, 1955).

[76] W. Israel, Singular hypersurfaces and thin shells in general relativity, Nuovo Cimento **44B,** 1 (1966); and corrections in **48B,** 463 (1966).

[77] E. F. Eiroa and G. E. Romero, Linearized stability of charged thin-shell wormholes, Gen. Relativ. Gravit. **36,** 651 (2004).

[78] F. S. N. Lobo and P. Crawford, Linearized stability analysis of thin shell wormholes with a cosmological constant, Classical Quantum Gravity **21,** 391 (2004).

[79] J. Fraundiener, C. Hoenselaers, and W. Konrad, A shell around a black hole, Classical Quantum Gravity **7,** 585 (1990).

[80] P. R. Brady, J. Louko, and E. Poisson, Stability of a shell around a black hole, Phys. Rev. D **44,** 1891 (1991).

[81] S. M. C. V. Gonćalves, Relativistic shells: Dynamics, horizons, and shell crossing, Phys. Rev. D **66,** 084021 (2002).

[82] J. P. S. Lemos, F. S. N. Lobo, and S. Q. de Oliveira, Morris-Thorne wormholes with a cosmological constant, Phys. Rev. D **68,** 064004 (2003).

[83] F. S. N. Lobo, Energy conditions, traversable wormholes and dust shells, Gen. Relativ. Gravit. **37,** 2023 (2005).

[84] F. S. N. Lobo, Surface stresses on a thin shell surrounding a traversable wormhole, Classical Quantum Gravity **21,** 4811 (2004).

[85] J. P. S. Lemos and F. S. N. Lobo, Plane symmetric traversable wormholes in an anti-de Sitter background, Phys. Rev. D **69,** 104007 (2004).

[86] S. Sushkov, Wormholes supported by a phantom energy, Phys. Rev. D **71,** 043520 (2005).

[87] F. S. N. Lobo, Phantom energy traversable wormholes, Phys. Rev. D **71,** 084011 (2005).

[88] F. S. N. Lobo and P. Crawford, Stability analysis of dynamic thin shells, Classical Quantum Gravity **22,** 4869 (2005).

[89] F. S. N. Lobo, Stability of phantom wormholes, Phys. Rev. D **71,** 124022 (2005).

[90] E. F. Eiroa and C. Simeone, Cylindrical thin shell wormholes, Phys. Rev. D **70,** 044008 (2004).

[91] E. F. Eiroa and C. Simeone, Thin-shell wormholes in dilaton gravity, Phys. Rev. D **71,** 127501 (2005).

[92] M. Thibeault, C. Simeone, and E. F. Eiroa, Thin-shell wormholes in Einstein-Maxwell theory with a Gauss-Bonnet term, Gen. Relativ. Gravit. **38,** 1593 (2006).

[93] F. Rahaman, M. Kalam, and S. Chakraborty, Thin shell wormholes in higher dimensional Einstein-Maxwell theory, Gen. Relativ. Gravit. **38,** 1687 (2006).

[94] F. Rahaman, M. Kalam, and S. Chakraborti, Thin shell wormhole in heterotic string theory, Int. J. Mod. Phys. D **16,** 1669 (2007).

[95] C. Bejarano, E. F. Eiroa, and C. Simeone, Thin-shell wormholes associated with global cosmic strings, Phys. Rev. D **75,** 027501 (2007).

[96] E. F. Eiroa and C. Simeone, Stability of Chaplygin gas thin-shell wormholes, Phys. Rev. D **76,** 024021 (2007).

[97] J. P. S. Lemos and F. S. N. Lobo, Plane symmetric thin-shell wormholes: Solutions and stability, Phys. Rev. D **78,** 044030 (2008).

[98] E. F. Eiroa, M. G. Richarte, and C. Simeone, Thin-shell wormholes in Brans–Dicke gravity, Phys. Lett. A **373,** 1 (2008); Erratum, Phys. Lett. A **373,** 2399 (2009).

[99] E. F. Eiroa, Thin-shell wormholes with a generalized Chaplygin gas, Phys. Rev. D **80,** 044033 (2009).

[100] E. F. Eiroa, Stability of thin-shell wormholes with spherical symmetry, Phys. Rev. D **78,** 024018 (2008).

[101] E. F. Eiroa and C. Simeone, Some general aspects of thin-shell wormholes with cylindrical symmetry, Phys. Rev. D **81,** 084022 (2010).

[102] S. H. Mazharimousavi, M. Halilsoy, and Z. Amirabi, Stability of thin-shell wormholes supported by ordinary matter in Einstein-Maxwell-Gauss-Bonnet gravity, Phys. Rev. D **81,** 104002 (2010).

[103] G. A. S. Dias and J. P. S. Lemos, Thin-shell wormholes in *d*-dimensional general relativity: Solutions, properties, and stability, Phys. Rev. D **82,** 084023 (2010).

[104] X. Yue and S. Gao, Stability of Brans-Dicke thin shell wormholes, Phys. Lett. A **375,** 2193 (2011).

[105] A. DeBenedictis, R. Garattini, and F. S. N. Lobo, Phantom stars and topology change, Phys. Rev. D **78,** 104003 (2008).

[106] P. Musgrave and K. Lake, Junctions and thin shells in general relativity using computer algebra I: The Darmois-Israel formalism, Classical Quantum Gravity **13,** 1885 (1996).

[107] M. Ishak and K. Lake, Stability of transparent spherically symmetric thin shells and wormholes, Phys. Rev. D **65,** 044011 (2002).

[108] S. W. Hawking and G. F. R. Ellis, *The Large Scale Structure of Spacetime* (Cambridge University Press, Cambridge, England, 1973).

[109] K. A. Bronnikov, V. N. Melnikov, and H. Dehnen, Regular black holes and black universes, Gen. Relativ. Gravit. **39,** 973 (2007).

[110] K. A. Bronnikov, V. N. Melnikov, and H. Dehnen, On a general class of brane world black holes, Phys. Rev. D **68,** 024025 (2003).

[111] P. O. Mazur and E. Mottola, Gravitational condensate stars: An alternative to black holes, arXiv:gr-qc/0109035.

[112] P. O. Mazur and E. Mottola, *10th Marcel Grossmann Meeting on Recent Developments in Theoretical and Experimental General Relativity, Gravitation and Relativistic Field Theories (MG X MMIII)* (World Scientific Publishing, Singapore, 2006), pp. 1041–1047.

[113] P. O. Mazur and E. Mottola, Dark energy and condensate stars: Casimir energy in the large, arXiv:gr-qc/0405111.

[114] P. O. Mazur and E. Mottola, Gravitational vacuum condensate stars, Proc. Natl. Acad. Sci. U.S.A. **101,** 9545 (2004).

[115] M. Visser and D. L. Wiltshire, Stable gravastars: An Alternative to black holes?, Classical Quantum Gravity **21,** 1135 (2004).

[116] C. Cattöen, T. Faber, and M. Visser, Gravastars must have anisotropic pressures, Classical Quantum Gravity **22,** 4189 (2005).

[117] F. S. N. Lobo, Stable dark energy stars, Classical Quantum Gravity **23,** 1525 (2006).

[118] F. S. N. Lobo and A. V. B. Arellano, Gravastars supported by nonlinear electrodynamics, Classical Quantum Gravity **24,** 1069 (2007).

[119] P. Martín-Moruno, N. Montelongo-García, F. S. N. Lobo, and M. Visser, Generic thin-shell gravastars, J. Cosmol. Astropart. Phys. 03 (2012) 034.

[120] F. S. N. Lobo, P. Martín-Moruno, N. Montelongo-García, and M. Visser, Novel stability approach of thin-shell gravastars, arXiv:1512.07659.